


# Broadband high contrast ratio optical diodes based on polarization conversion

Xiaohu Wu<sup>1</sup> · Ceji Fu<sup>1</sup> 

Received: 3 May 2017 / Accepted: 28 August 2017 / Published online: 8 September 2017  
© Springer-Verlag GmbH Germany 2017

**Abstract** We propose an alternative method to realize broadband high contrast ratio optical diodes based on polarization conversion between transverse electric (TE) wave and transverse magnetic (TM) wave with two slabs of uniaxial hyperbolic crystal. Taking hexagonal boron nitride as an example of the crystal, our numerical simulation results show that asymmetric transmission can occur in the wavelength range from 6.40 to 7.38  $\mu\text{m}$  for incidence of a TM wave, and the transmissivity contrast ratio can be beyond 1000 in the wavelength range from 6.63 to 7.33  $\mu\text{m}$ . For incidence of a TE wave, the asymmetric transmission with the transmissivity contrast ratio higher than 1000 is found in the wavelength range from 12.33 to 12.88  $\mu\text{m}$ . Given that the structure is novel and simple, it may provide a promising prototype for designing high performance integrated photonic devices, such as optical logic gate and optical memory.

## 1 Introduction

Optical diodes have attracted great attention due to their vital applications in information processing and optical computing systems [1–3]. An optical diode allows light to transmit only in one direction while blocking it in the opposite direction [4]. Many different mechanisms and methods have been proposed to realize optical diode up to now, and the most commonly used methods are based on

the magneto-optical effect [5–8] and nonlinearity [9–15]. However, the magneto-optical effect usually needs a strong external magnetic field, which is incompatible with compact integrated devices. In addition, the high threshold of nonlinear effect would limit its practical usage. Other linear methods include depositing a metal film with nanohole arrays in it on the surface of a photonic crystal (PC) [16] and using a two-dimensional air-hole PC waveguide [17]. High contrast ratio and large operating bandwidth are two key characteristics for optical diodes [1]. Lots of effort has been made to improve the performance of optical diodes, such as using Fano resonance [4], Dirac cone [18], pump-assisted PC resonator [19] and metallic PC [20]. These methods require the use of different PC structures. Hwang [21] and Song [22] reported an optical diode device by using the photonic bandgap effect for different circularly polarized lights without adopting any optical nonlinearity. Nevertheless, their device cannot obtain high contrast ratio. In this paper, we propose to realize a broadband high contrast ratio optical diode based on polarization conversion in the absence of nonlinearity and PC structures.

We consider in this work a structure containing only two uniaxial crystal slabs. One of them is used to manipulate the polarization status between transverse electric (TE) wave and transverse magnetic (TM) wave, and the other one is used to bring out selective reflection and transmission for different polarized waves. Combining these two effects together, we show that it is possible to achieve effectively a broadband high contrast ratio optical diode. It should be noted that the term “optical diode” we refer to here is associated with asymmetric transmission of the structure, which is different from those based on an optical isolator [23] because the system we are studying is reciprocal. In the following we will analyze the working mechanism and performance of the optical diode.

✉ Ceji Fu  
cjfu@pku.edu.cn

<sup>1</sup> LTCS and Department of Mechanics and Engineering Science, College of Engineering, Peking University, Beijing 100871, China

## 2 Model and theoretical methods

We take hexagonal boron nitride (hBN) as the uniaxial crystal in this work. The structure is illustrated in Fig. 1a. The optical axis of hBN is first taken to be parallel to the  $y$ -axis of the coordinate system  $xyz$ . In this case, the permittivity tensor of the uniaxial crystal can be described by the Lorentz model as [24]:

$$\begin{aligned} \boldsymbol{\varepsilon} &= \begin{pmatrix} \varepsilon_{\perp} & 0 & 0 \\ 0 & \varepsilon_{\parallel} & 0 \\ 0 & 0 & \varepsilon_{\perp} \end{pmatrix}, \varepsilon_m \\ &= \varepsilon_{\infty,m} \left( 1 + \frac{\omega_{LO,m}^2 - \omega_{TO,m}^2}{\omega_{TO,m}^2 - \omega^2 + j\omega\Gamma_m} \right), \end{aligned} \quad (1)$$

where  $j$  is the imaginary unit and  $m = \perp, \parallel$  indicates the component perpendicular or parallel to the optical axis.  $\omega$  is the wavenumber, the other parameters are  $\omega_{TO,\perp} = 1370 \text{ cm}^{-1}$ ,  $\omega_{TO,\parallel} = 780 \text{ cm}^{-1}$ ,  $\omega_{LO,\perp} = 1610 \text{ cm}^{-1}$ ,  $\omega_{LO,\parallel} = 830 \text{ cm}^{-1}$ ,  $\varepsilon_{\infty,\perp} = 4.87$ ,  $\varepsilon_{\infty,\parallel} = 2.95$ ,  $\Gamma_{\perp} =$

$5 \text{ cm}^{-1}$  and  $\Gamma_{\parallel} = 4 \text{ cm}^{-1}$ . Figure 1b shows the real parts of  $\varepsilon_{\perp}$  and  $\varepsilon_{\parallel}$  in the wavelength range from 6 to 14  $\mu\text{m}$ . It can be seen that  $\text{Re}(\varepsilon_{\perp})$  has a sharp change from a large negative value to a large positive value at wavelength 7.3  $\mu\text{m}$  (corresponding to  $\omega_{TO,\perp}$ ), while  $\text{Re}(\varepsilon_{\parallel})$  stays at the value of  $\varepsilon_{\infty,\parallel}$  in the wavelength range around 7.3  $\mu\text{m}$ . On the other hand,  $\text{Re}(\varepsilon_{\parallel})$  has a sharp change from a large negative value to a large positive value at wavelength 12.82  $\mu\text{m}$  (corresponding to  $\omega_{TO,\parallel}$ ), while  $\text{Re}(\varepsilon_{\perp})$  stays at the value of  $\varepsilon_{\infty,\perp}$  in the wavelength range around 12.82  $\mu\text{m}$ . In the two bands of wavelength lower than 7.3 and 12.82  $\mu\text{m}$ ,  $\text{Re}(\varepsilon_{\parallel})$  and  $\text{Re}(\varepsilon_{\perp})$  have opposite signs, and the dispersion relation of a TM wave propagation in the medium is hyperbolic in these two bands, respectively. Therefore, the medium can be termed a hyperbolic medium [25]. The two hyperbolic bands of hBN make the slab exhibiting very different reflection and transmission phenomena for an electromagnetic wave of different polarizations incident on it, as will be discussed.

Now rotating the top slab around the  $z$ -axis by an angle  $\phi$ , we get a new permittivity tensor for this slab in the  $xyz$  coordinate system as

$$\boldsymbol{\varepsilon} = \begin{pmatrix} \varepsilon_{xx} & \varepsilon_{xy} & 0 \\ \varepsilon_{yx} & \varepsilon_{yy} & 0 \\ 0 & 0 & \varepsilon_{zz} \end{pmatrix}, \quad (2)$$

where  $\varepsilon_{xx} = \varepsilon_{\parallel} + (\varepsilon_{\perp} - \varepsilon_{\parallel}) \cos^2 \phi$ ,  $\varepsilon_{xy} = \varepsilon_{yx} = 0.5 (\varepsilon_{\perp} - \varepsilon_{\parallel}) \sin 2\phi$ ,  $\varepsilon_{yy} = \varepsilon_{\parallel} + (\varepsilon_{\perp} - \varepsilon_{\parallel}) \sin^2 \phi$  and  $\varepsilon_{zz} = \varepsilon_{\perp}$ . The coordinate system  $x_1y_1z_1$  shown in Fig. 1a is the system fixed to the top slab such that its  $y_1$ -axis is parallel to the slab's optical axis. In other words, the angle between the  $x$ -axis and the  $x_1$ -axis of the two coordinate systems is equal to  $\phi$ . In this work, our analysis is based on the  $xyz$  coordinate system. We assume normal incidence of a plane wave on the structure and the  $x$ - $z$  plane is the plane of incidence. In this case, the incident wave is a TE wave if its electric field is along the  $y$ -axis while it is a TM wave if its magnetic field is along the  $y$ -axis. In the crystal, the electromagnetic fields can be expressed in the following form [26],

$$\mathbf{E} = \mathbf{S}(z) \exp(j\omega t), \mathbf{S}(z) = (S_x, S_y, 0), \quad (3)$$

$$\mathbf{H} = -j \left( \frac{\varepsilon_0}{\mu_0} \right)^{1/2} \mathbf{U}(z) \exp(j\omega t), \mathbf{U}(z) = (U_x, U_y, 0), \quad (4)$$

where  $\varepsilon_0$  and  $\mu_0$  are the permittivity and the permeability of vacuum. The vectors  $\mathbf{S}$  and  $\mathbf{U}$  denote the magnitude and direction of the electric and the magnetic fields, respectively. Substituting Eqs. (3) and (4) into the Maxwell equations and setting  $z' = z\omega\sqrt{\varepsilon_0\mu_0}$ , we get the following differential equations [26]

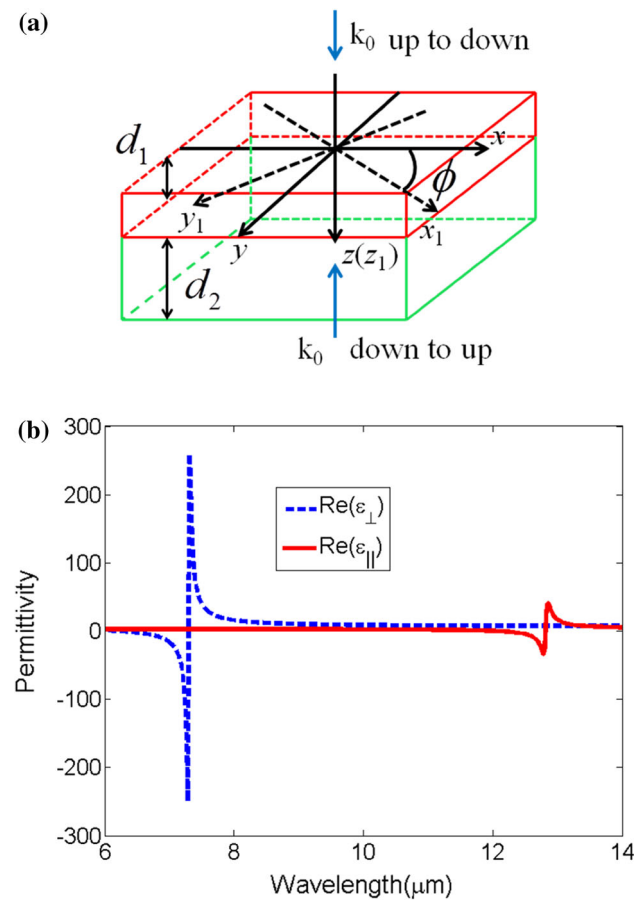


**Fig. 1** **a** Schematic of the structure and the coordinate systems, rotation of  $xyz$  by an angle  $\phi$  around the  $z$ -axis to get  $x_1y_1z_1$ . The thickness of the top and the bottom slabs are  $d_1$  and  $d_2$ , respectively. **b** The real parts of  $\varepsilon_{\perp}$  and  $\varepsilon_{\parallel}$  of hBN variation with wavelength

$$\frac{d}{dz'} \begin{pmatrix} S_x \\ S_y \\ U_x \\ U_y \end{pmatrix} = \mathbf{A} \begin{pmatrix} S_x \\ S_y \\ U_x \\ U_y \end{pmatrix}, \quad \mathbf{A} = \begin{pmatrix} 0 & 0 & 0 & -1 \\ 0 & 0 & 1 & 0 \\ -\varepsilon_{xy} & -\varepsilon_{yy} & 0 & 0 \\ \varepsilon_{xx} & \varepsilon_{xy} & 0 & 0 \end{pmatrix}, \tag{5}$$

From the coefficient matrix  $\mathbf{A}$ , it can be seen that TE wave and TM wave couple together and conversion of polarization can occur if  $\varepsilon_{xy} \neq 0$ . But when  $\varepsilon_{xy} = 0$ , i.e., when the rotation angle  $\phi = 0^\circ$ , Eq. (5) can be decomposed into

$$\frac{d}{dz'} \begin{pmatrix} S_x \\ U_y \end{pmatrix} = \begin{pmatrix} 0 & -1 \\ \varepsilon_{\perp} & 0 \end{pmatrix} \begin{pmatrix} S_x \\ U_y \end{pmatrix}, \tag{6}$$

and

$$\frac{d}{dz'} \begin{pmatrix} S_y \\ U_x \end{pmatrix} = \begin{pmatrix} 0 & 1 \\ -\varepsilon_{\parallel} & 0 \end{pmatrix} \begin{pmatrix} S_y \\ U_x \end{pmatrix}, \tag{7}$$

Equations (6) and (7) indicate that TM wave and TE wave are decoupled and they can be solved separately. In this case, the propagation of a TM wave in the slab is only related to  $\varepsilon_{\perp}$  while the propagation of a TE wave in the slab is only related to  $\varepsilon_{\parallel}$ . Therefore, incidence of a TM wave on an hBN slab will have different reflection and transmission from incidence of a TE wave, and there is no conversion of polarization between them. In the following, we focus our attention on the hyperbolic bands, in which the optical response for TE and TM waves can be significantly different due to the opposite signs of  $\text{Re}(\varepsilon_{\parallel})$  and  $\text{Re}(\varepsilon_{\perp})$ . Figures 2a and 2b show respectively the calculated reflectivity and transmissivity of an hBN slab of thickness equal to  $2 \mu\text{m}$ , whose permittivity tensor is in the form of Eq. (1), for normal incidence of TE and TM waves in the wavelength range from  $6.16$  to  $7.4 \mu\text{m}$ . It can be seen from Fig. 2a that the reflectivity is close to zero for incidence of TE wave while the reflectivity is high for incidence of TM wave in the whole specified wavelength range. Especially the reflectivity for the latter is close to unity in the wavelength range from  $6.4$  to  $7.3 \mu\text{m}$ . Figure 2b shows that the transmissivity for incidence of TE wave is close to unity in the whole specified wavelength range. However, the transmissivity for incidence of TM wave is almost zero in the wavelength range from  $6.4$  to  $7.4 \mu\text{m}$ . These different reflection and transmission phenomena for incidence of TE and TM waves on the slab are important factors, though not sufficient, for realizing the optical diode. Furthermore, it can be found from Fig. 2 that absorption in the hBN slab is very small, since hBN is a low-loss material [27, 28].

We investigate the transmissivity of the structure shown in Fig. 1a with the top slab rotated around the  $z$ -axis by an angle  $\phi$  while the bottom slab remains intact. In doing so, we extended the traditional enhanced transmittance matrix approach [26, 29] to permit conversion of polarization and

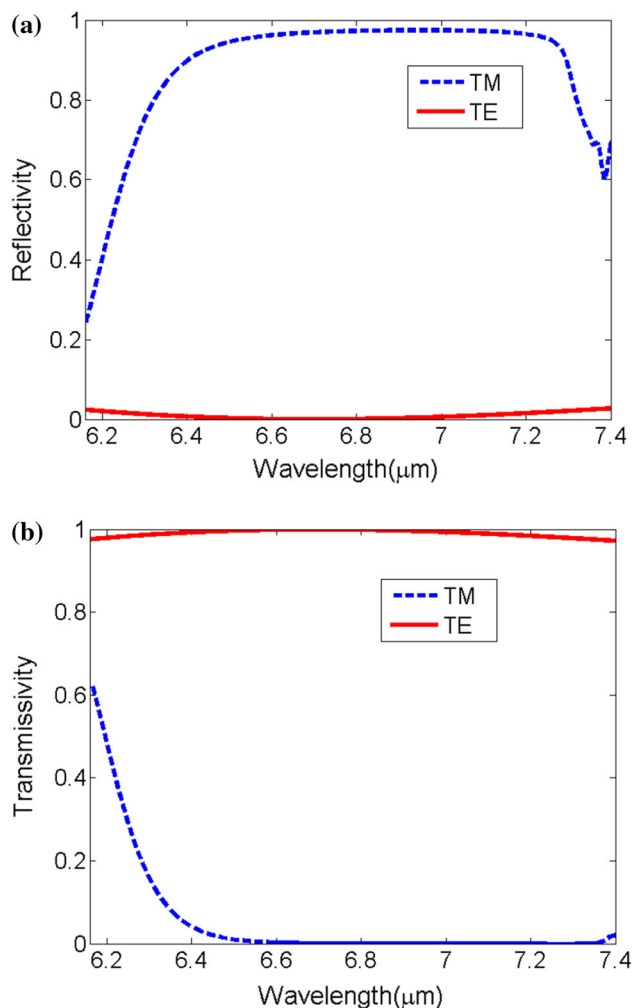


**Fig. 2** a Reflectivity as a function of wavelength for TM wave and TE wave. b Transmissivity as a function of wavelength for TM wave and TE wave

applied it to calculate the electromagnetic fields inside the slabs. With this method, we express the electromagnetic fields in terms of the eigenvalues and eigenvectors of matrix  $\mathbf{A}$  shown in Eq. (5) and solve for the reflection and transmission coefficients by matching the tangential field components at each interface. Furthermore, an algorithm that can avoid the problem of numerical overflow in using the transfer matrix method was also adopted. For brevity, the detailed derivation of the reflectivity and the transmissivity of the structure is put in the Appendix and only the results are discussed here.

### 3 Results and discussion

In order to realize the transmissivity characteristic of an optical diode, conversion of polarization by using the top hBN slab is required in the structure. For the purpose of

achieving maximum conversion efficiency between TM wave and TE wave, the rotation angle is set as  $\phi = 45^\circ$  [26]. On the other hand, the conversion efficiency depends on the thickness of the top slab, which should be taken to ensure large transmission of the converted wave through the top slab. For the bottom slab, its thickness should be taken to ensure that the slab block a TM (or TE) wave while permitting large transmission of a TE (or TM). Here, we first consider incidence of a TM wave, and the thicknesses of the top and the bottom slabs are taken by optimization to be 1 and 2  $\mu\text{m}$ , respectively. Figure 3a shows the calculated transmissivity of the structure for the TM wave incident from the top and from the bottom, respectively. It can be seen that the incidence cannot pass the structure from the bottom slab to the top slab in the wavelength range from 6.40 to 7.38  $\mu\text{m}$ , while the

incidence can pass the structure from the opposite direction. In order for better understanding the underlying mechanism, we define  $T_{pp}$  and  $T_{ps}$  as the transmissivity of the unconverted TM wave component and the TE wave component converted from TM wave, respectively. Figure 3b shows the calculated  $T_{pp}$  and  $T_{ps}$  for incidence from the opposite directions. As shown, the incident TM wave from the top can be partly converted to TE wave in the top slab. This TE wave can then pass the bottom slab while the unconverted TM wave is blocked by the bottom slab in the wavelength range from 6.40 to 7.38  $\mu\text{m}$ . Therefore, the total transmissivity is not zero and is contributed from the converted TE wave. In contrast, when the TM wave is incident from the bottom, it cannot pass the bottom slab, thus leading to nearly zero total transmission. As a consequence, an optical diode in a broad band is realized with the structure.

Another key characteristic for an optical diode is the transmissivity contrast ratio (TCR), which is defined as  $T_1/T_2$ , where  $T_1$  is the transmissivity for incidence from the top and  $T_2$  is the transmissivity for incidence from the opposite direction. Figure 4 shows the TCR for normal incidence of a TM wave from the top and from the bottom varying with wavelength, a value beyond 1000 is revealed in the wavelength range from 6.63 to 7.33  $\mu\text{m}$ . The maximum TCR can reach  $10^{26}$ , which is much larger than the best available value in published literature [18].

The high TCR of the optical diode shown in Fig. 4 stems from the hyperbolicity of hBN. In the hyperbolic band of hBN from 6.4 to 7.3  $\mu\text{m}$ , the real part of  $\epsilon_\perp$  is negative while the real part of  $\epsilon_\parallel$  is positive. In the bottom slab, the propagation of TM wave is only related to  $\epsilon_\perp$  while the propagation of TE wave is only related to  $\epsilon_\parallel$ . Therefore, the TM wave cannot pass the bottom slab while

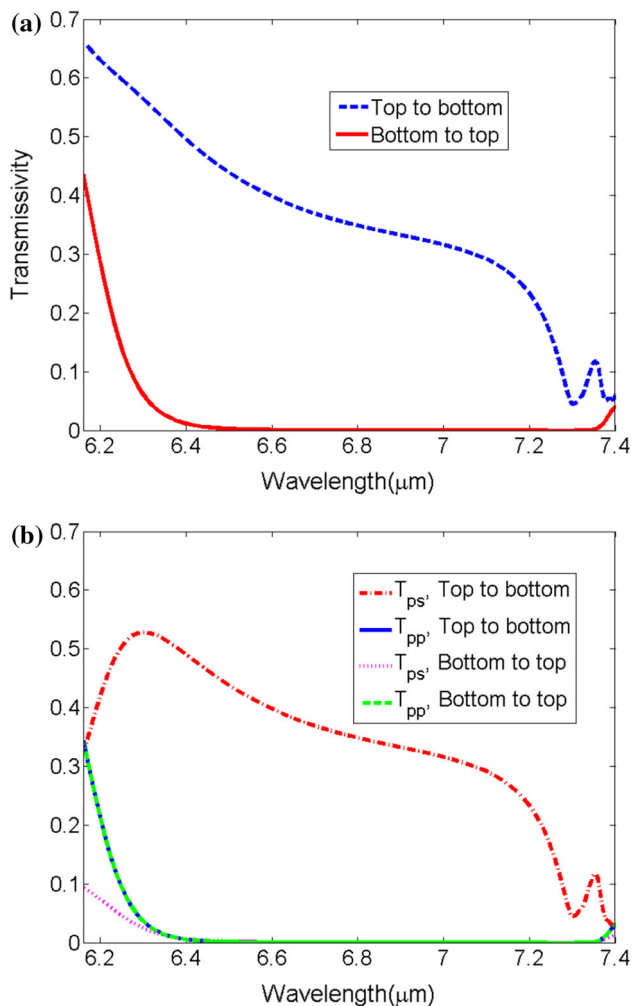


**Fig. 3** **a** Transmissivity as a function of wavelength for normal incidence of a TM wave in two opposite directions. **b** Transmissivity of the unconverted TM wave component and the converted TE wave component for normal incidence of a TM wave from two opposite directions

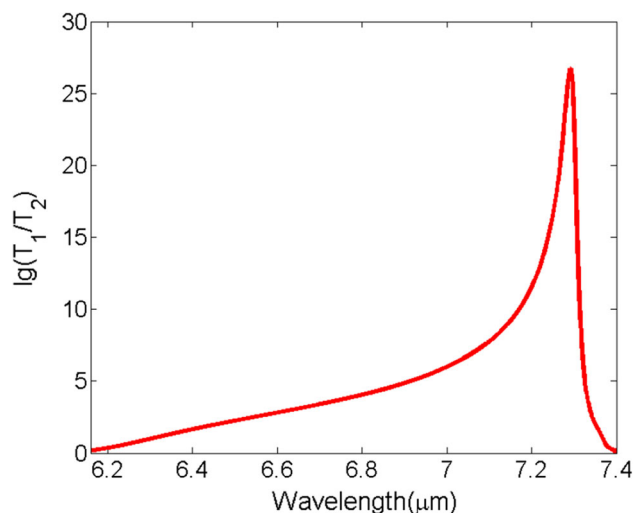


**Fig. 4** Transmissivity contrast ratio for normal incidence of a TM wave from two opposite directions as a function of wavelength

the TE wave can. This is the cause for the high TCR of the optical diode. We should emphasize that an optical diode can also be realized when the real part of  $\epsilon_{\perp}$  and  $\epsilon_{\parallel}$  share the same sign. However, a high TCR is hard to obtain in that case. This explains why a hyperbolic material should be selected for making the optical diode of high contrast ratio.

Likewise, an optical diode can also be achieved for incidence of a TE wave by using the proposed structure, but in a different wavelength range. In this case, the thickness of the top slab is remained to be 1  $\mu\text{m}$  but the thickness of the bottom slab is changed to 6  $\mu\text{m}$ . Figure 5a shows that there is almost no transmission in the wavelength range from 12.2 to 12.9  $\mu\text{m}$  when the TE wave is normally incident from below, while the transmissivity is higher than 0.2 in the whole wavelength range of interest for incidence from the opposite direction. Figure 5b

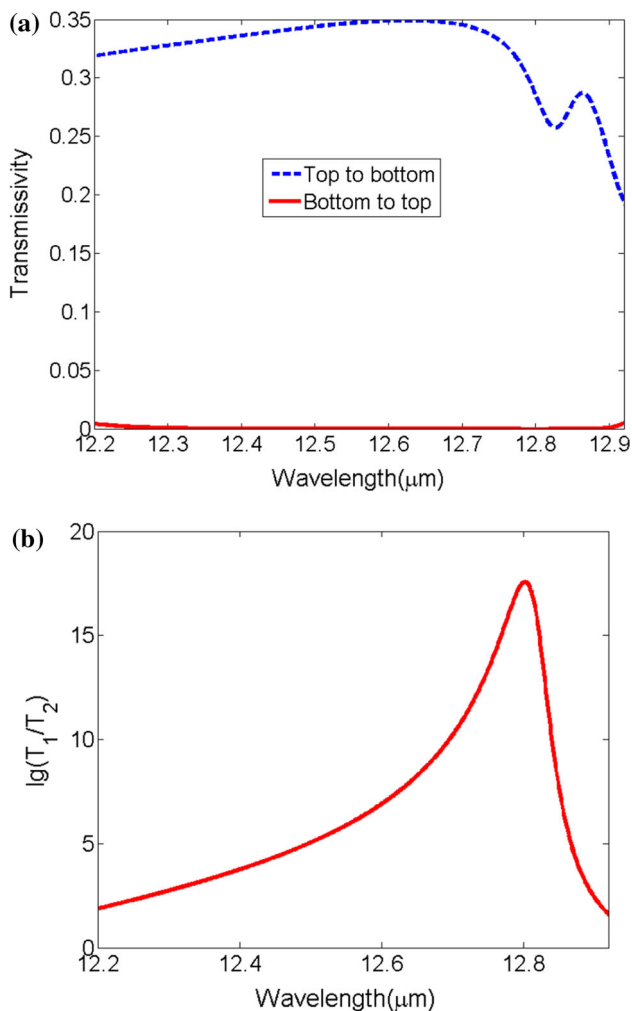


**Fig. 5** **a** Transmissivity as a function of wavelength for normal incidence of a TE wave from two opposite directions. **b** Transmissivity contrast ratio for normal incidence of a TE wave from two opposite directions as a function of wavelength

illustrates the TCR varying with wavelength for normal incidence of the TE wave from the two opposite directions. A waveband is found from 12.33 to 12.88  $\mu\text{m}$  for the TCR higher than 1000. Furthermore, the maximum TCR at 12.8  $\mu\text{m}$  is higher than  $10^{17}$ . The underlying mechanism is similar to that for incidence of TM wave. When the incident TE wave is from the top, it can be partly converted to TM wave in the top slab, which can pass the bottom slab, thus the total transmissivity is not zero and is contributed from the converted TM wave. But when the incident TE wave is from below, it is blocked by the bottom slab, thus leading to a nearly zero total transmissivity.

It should be pointed out that although our above analysis is based on a natural hyperbolic crystal hBN, on which the obtained wavebands for an optical diode are not tunable, this setback can be overcome by replacing the hBN slabs with hyperbolic metamaterial slabs. Because a hyperbolic metamaterial is an artificial uniaxial crystal, whose hyperbolic waveband can be tailored by tuning the geometric parameters of the metamaterial [25]. Therefore, with the structure made of hyperbolic metamaterial slabs, it is possible to realize an optical diode in a targeted waveband by properly tuning the geometric parameters of the metamaterial.

### 4 Conclusions

In short, we propose a simple method to realize a broadband optical diode with high contrast ratio based on polarization conversion between TE wave and TM wave with a two-layer structure made of hBN. Numerical simulation results show that an optical diode can be achieved with TCR higher than 1000 in the wavelength range from 6.63 to 7.33  $\mu\text{m}$  for incidence of a TM wave. For incidence of a TE wave, an optical diode is also found in the wavelength range from 12.33 to 12.88  $\mu\text{m}$  with TCR higher than 1000. Furthermore, the maximum TCR can be much higher than the values in published literature. We conclude that the proposed simple structure is promising for high performance integrated photonic devices, such as optical logic gate and optical memory.

**Acknowledgements** This work was supported by the National Natural Science Foundation of China (Grant No. 51576004).

### Appendix

This appendix is dealing with the calculation of the reflection and transmission coefficients of multilayered structures where conversion of polarization between transverse magnetic wave (TM) and transverse electric (TE) wave can occur.

We first consider a simple case that the structure consists of only one hBN slab of thickness  $d$ . The electromagnetic field vector components in the slab can be expressed as

$$S_x(z) = \sum_{m=1}^2 w_{1,m} c_m^+ \exp(-k_0 q_m z) + \sum_{m=1}^2 w_{1,m+2} c_m^- \exp[k_0 q_m (z - d)], \tag{8}$$

$$S_y(z) = \sum_{m=1}^2 w_{2,m} c_m^+ \exp(-k_0 q_m z) + \sum_{m=1}^2 w_{2,m+2} c_m^- \exp[k_0 q_m (z - d)], \tag{9}$$

$$U_x(z) = \sum_{m=1}^2 w_{3,m} c_m^+ \exp(-k_0 q_m z) + \sum_{m=1}^2 w_{3,m+2} c_m^- \exp[k_0 q_m (z - d)], \tag{10}$$

$$U_y(z) = \sum_{m=1}^2 w_{4,m} c_m^+ \exp(-k_0 q_m z) + \sum_{m=1}^2 w_{4,m+2} c_m^- \exp[k_0 q_m (z - d)], \tag{11}$$

where  $w_{i,m}$  are the elements of the eigenvector matrix  $\mathbf{W}$  of matrix  $\mathbf{A}$  in Eq. (5).  $-q_m$  and  $q_m$  are the eigenvalues of matrix  $\mathbf{A}$ , and the real part of  $q_m$  is positive.  $c_m^+$  and  $c_m^-$  are unknowns, and can be determined by applying the boundary conditions. Supposing incidence of a TM wave, we calculate the reflection and transmission coefficients by matching the tangential electric and magnetic field components at the boundaries. At the top surface ( $z = 0$ )

$$\begin{pmatrix} -j \\ 0 \\ 0 \\ 1 \end{pmatrix} + \begin{pmatrix} j & 0 \\ 0 & -j \\ 0 & 1 \\ 1 & 0 \end{pmatrix} \begin{bmatrix} r_{pp} \\ r_{ps} \end{bmatrix} = [\mathbf{W}_{11} \quad \mathbf{W}_{12} \mathbf{X}] \begin{bmatrix} \mathbf{C}^+ \\ \mathbf{C}^- \end{bmatrix}, \tag{12}$$

and at the bottom surface ( $z = d$ )

$$[\mathbf{W}_{11} \mathbf{X} \quad \mathbf{W}_{12}] \begin{bmatrix} \mathbf{C}^+ \\ \mathbf{C}^- \end{bmatrix} = \begin{pmatrix} -j & 0 \\ 0 & -j \\ 0 & -1 \\ 1 & 0 \end{pmatrix} \begin{bmatrix} t_{pp} \\ t_{ps} \end{bmatrix}, \tag{13}$$

where  $\mathbf{X}$  is a diagonal matrix with the diagonal elements as  $\exp(-k_0 q_m d)$ .  $\mathbf{W}_{11}$  and  $\mathbf{W}_{12}$  are two partitioned matrices of  $\mathbf{W}$ ,  $\mathbf{W} = [\mathbf{W}_{11} \quad \mathbf{W}_{12}]$ .  $\mathbf{C}^+$  and  $\mathbf{C}^-$  are vectors composed of the unknowns  $c_m^+$  and  $c_m^-$ .  $r_{pp}$  and  $r_{ps}$  are the reflection coefficients for TM and TE waves, respectively. Similarly,  $t_{pp}$  and  $t_{ps}$  are the transmission coefficients for TM and TE

waves, respectively. These four coefficients can be obtained by solving Eqs. (12) and (13). Now we extend the above analysis to an arbitrary  $L$ -layer structure by matching the tangential electric and magnetic field components at each interface. The following equations are then obtained

$$\begin{pmatrix} -j \\ 0 \\ 0 \\ 1 \end{pmatrix} + \begin{pmatrix} j & 0 \\ 0 & -j \\ 0 & 1 \\ 1 & 0 \end{pmatrix} \begin{bmatrix} r_{pp} \\ r_{ps} \end{bmatrix} = [\mathbf{W}_{(1)1} \quad \mathbf{W}_{(1)2} \mathbf{X}_{(1)}] \begin{bmatrix} \mathbf{C}_{(1)}^+ \\ \mathbf{C}_{(1)}^- \end{bmatrix}, \tag{14}$$

$$[\mathbf{W}_{(l-1)1} \mathbf{X}_{(l-1)} \quad \mathbf{W}_{(l-1)2}] \begin{bmatrix} \mathbf{C}_{(l-1)}^+ \\ \mathbf{C}_{(l-1)}^- \end{bmatrix} = [\mathbf{W}_{(l)1} \quad \mathbf{W}_{(l)2} \mathbf{X}_{(l)}] \begin{bmatrix} \mathbf{C}_{(l)}^+ \\ \mathbf{C}_{(l)}^- \end{bmatrix}, \tag{15}$$

$$[\mathbf{W}_{(L)1} \mathbf{X}_{(L)} \quad \mathbf{W}_{(L)2}] \begin{bmatrix} \mathbf{C}_{(L)}^+ \\ \mathbf{C}_{(L)}^- \end{bmatrix} = \begin{pmatrix} -j & 0 \\ 0 & -j \\ 0 & -1 \\ 1 & 0 \end{pmatrix} \begin{bmatrix} t_{pp} \\ t_{ps} \end{bmatrix}, \tag{16}$$

where  $l = 2, 3, \dots, L$ .  $\mathbf{W}_{(l)}$  and  $\mathbf{X}_{(l)}$  have the same definition as  $\mathbf{W}$  and  $\mathbf{X}$  described above. For each  $l$ ,  $\mathbf{W}_{(l)} = [\mathbf{W}_{(l)1} \quad \mathbf{W}_{(l)2}]$ . To preempt the numerical instability associated with the inversion of the matrix, we propose to adopt the enhanced transmittance matrix approach. From Eq. (16), one has

$$\begin{bmatrix} \mathbf{C}_{(L)}^+ \\ \mathbf{C}_{(L)}^- \end{bmatrix} = [\mathbf{W}_{(L)1} \mathbf{X}_{(L)} \quad \mathbf{W}_{(L)2}]^{-1} \begin{pmatrix} -j & 0 \\ 0 & -j \\ 0 & -1 \\ 1 & 0 \end{pmatrix} \begin{bmatrix} t_{pp} \\ t_{ps} \end{bmatrix} = [\mathbf{W}_{(L)1} \mathbf{X}_{(L)} \quad \mathbf{W}_{(L)2}]^{-1} \begin{pmatrix} \mathbf{f}_{L+1} \\ \mathbf{g}_{L+1} \end{pmatrix} \mathbf{t}, \tag{17}$$

where  $\mathbf{t} = \begin{bmatrix} t_{pp} \\ t_{ps} \end{bmatrix}$ ,  $\mathbf{f}_{L+1} = \begin{bmatrix} -j & 0 \\ 0 & -j \end{bmatrix}$  and  $\mathbf{g}_{L+1} = \begin{bmatrix} 0 & -1 \\ 1 & 0 \end{bmatrix}$ .

In order to ensure that the matrix to be inverted is numerically stable, we follow the procedure in [29] and rewrite it as the product of two matrices

$$[\mathbf{W}_{(L)1} \mathbf{X}_{(L)} \quad \mathbf{W}_{(L)2}]^{-1} = \begin{bmatrix} \mathbf{X}_{(L)} & 0 \\ 0 & \mathbf{I} \end{bmatrix}^{-1} [\mathbf{W}_{(L)1} \quad \mathbf{W}_{(L)2}]^{-1}. \tag{18}$$

The matrix on the right in the product is well conditioned, and its inversion is numerically stable [29]. Therefore, Eq. (17) can be rearranged as

$$\begin{bmatrix} \mathbf{C}_{(L)}^+ \\ \mathbf{C}_{(L)}^- \end{bmatrix} = \begin{bmatrix} \mathbf{X}_{(L)} & 0 \\ 0 & \mathbf{I} \end{bmatrix}^{-1} \begin{pmatrix} \mathbf{a}_L \\ \mathbf{b}_L \end{pmatrix} \mathbf{t}, \tag{19}$$

where  $\mathbf{I}$  is the unit matrix and

$$\begin{bmatrix} \mathbf{a}_L \\ \mathbf{b}_L \end{bmatrix} = [\mathbf{W}_{(L)1} \quad \mathbf{W}_{(L)2}]^{-1} \begin{bmatrix} \mathbf{f}_{L+1} \\ \mathbf{g}_{L+1} \end{bmatrix}.$$

The matrix to be inverted in Eq. (19) is ill conditioned when the elements of the diagonal matrix  $\mathbf{X}_{(L)}$  are very small, but we can perform the inversion analytically to obtain the inverted matrix. Furthermore, in order to avoid the problem that the diagonal elements cannot be represented with sufficient numerical accuracy because of the finite precision and the truncation errors, we adopt the substitution  $\mathbf{t} = \mathbf{a}_L^{-1} \mathbf{X}_L \mathbf{t}_L$  such that Eq. (19) becomes

$$\begin{bmatrix} \mathbf{C}_{(L)}^+ \\ \mathbf{C}_{(L)}^- \end{bmatrix} = \begin{pmatrix} \mathbf{I} \\ \mathbf{b}_L \mathbf{a}_L^{-1} \mathbf{X}_L \end{pmatrix} \mathbf{t}_L. \tag{20}$$

Putting Eq. (20) into Eq. (15) for  $l = L$ , we have

$$\begin{bmatrix} \mathbf{C}_{(L-1)}^+ \\ \mathbf{C}_{(L-1)}^- \end{bmatrix} = [\mathbf{W}_{(L-1)1} \mathbf{X}_{(L-1)} \quad \mathbf{W}_{(L-1)2}]^{-1} \begin{pmatrix} \mathbf{f}_L \\ \mathbf{g}_L \end{pmatrix} \mathbf{t}_L, \tag{21}$$

where

$$\begin{bmatrix} \mathbf{f}_L \\ \mathbf{g}_L \end{bmatrix} = (\mathbf{W}_{(L)1} + \mathbf{W}_{(L)2} \mathbf{X}_{(L)} \mathbf{b}_L \mathbf{a}_L^{-1} \mathbf{X}_{(L)}).$$

Repeating the above process for all layers, we obtain an equation of the form

$$\begin{pmatrix} -j \\ 0 \\ 0 \\ 1 \end{pmatrix} + \begin{bmatrix} j & 0 \\ 0 & -j \\ 0 & 1 \\ 1 & 0 \end{bmatrix} \mathbf{r} = \begin{bmatrix} \mathbf{f}_1 \\ \mathbf{g}_1 \end{bmatrix} \mathbf{t}_1, \tag{22}$$

where  $\mathbf{r} = \begin{bmatrix} r_{pp} \\ r_{ps} \end{bmatrix}$ .

We can solve Eq. (22) for  $\mathbf{r}$  and  $\mathbf{t}_1$ , then the transmission coefficient vector  $\mathbf{t}$  can be obtained as

$$\mathbf{t} = \mathbf{a}_L^{-1} \mathbf{X}_L \dots \mathbf{a}_1^{-1} \mathbf{X}_1 \dots \mathbf{t}_1. \tag{23}$$

Because the structure is bound by air, the reflectivity and transmissivity can be simply calculated as

$$R_{pp} = |r_{pp}|^2, R_{ps} = |r_{ps}|^2, T_{pp} = |t_{pp}|^2, T_{ps} = |t_{ps}|^2. \tag{24}$$

If the incidence is a TE wave, the process is basically the same as above. The solution can also be written as Eq. (A1), and the boundary conditions are

$$\begin{pmatrix} 0 \\ 1 \\ -j \\ 0 \end{pmatrix} + \begin{pmatrix} 1 & 0 \\ 0 & 1 \\ 0 & j \\ -j & 0 \end{pmatrix} \begin{bmatrix} r_{sp} \\ r_{ss} \end{bmatrix} = [\mathbf{W}_{(1)1} \quad \mathbf{W}_{(1)2} \mathbf{X}_{(1)}] \begin{bmatrix} \mathbf{C}_{(1)}^+ \\ \mathbf{C}_{(1)}^- \end{bmatrix}, \tag{25}$$

$$\begin{aligned} & [\mathbf{W}_{(l-1)1} \mathbf{X}_{(l-1)} \quad \mathbf{W}_{(l-1)2}] \begin{bmatrix} \mathbf{C}_{(l-1)}^+ \\ \mathbf{C}_{(l-1)}^- \end{bmatrix} \\ &= [\mathbf{W}_{(l)1} \quad \mathbf{W}_{(l)2} \mathbf{X}_{(l)}] \begin{bmatrix} \mathbf{C}_{(l)}^+ \\ \mathbf{C}_{(l)}^- \end{bmatrix}, \end{aligned} \tag{26}$$

$$[\mathbf{W}_{(L)1} \mathbf{X}_{(L)} \quad \mathbf{W}_{(L)2}] \begin{bmatrix} \mathbf{C}_{(L)}^+ \\ \mathbf{C}_{(L)}^- \end{bmatrix} = \begin{pmatrix} -1 & 0 \\ 0 & 1 \\ 0 & -j \\ -j & 0 \end{pmatrix} \begin{bmatrix} t_{sp} \\ t_{ss} \end{bmatrix}. \tag{27}$$

Following the process of Eq. (17) to Eq. (23), we can obtain the reflection and transmission coefficients  $r_{sp}$ ,  $r_{ss}$ ,  $t_{sp}$  and  $t_{ss}$ . The reflectivity and transmissivity can then be calculated as

$$R_{sp} = |r_{sp}|^2, R_{ss} = |r_{ss}|^2, T_{sp} = |t_{sp}|^2, T_{ss} = |t_{ss}|^2. \tag{28}$$

### References

1. C.C. Lu, X.Y. Hu, H. Yang, Q.H. Gong, *Opt. Lett.* **36**, 4668 (2011)
2. L. Fan, J. Wang, L.T. Varghese, H. Shen, B. Niu, Y. Xuan, A.M. Weiner, M. Qi, *Science* **335**, 447 (2012)
3. X.Y. Hu, Y.B. Zhang, X.N. Xu, Q.H. Gong, *Plasmonics* **6**, 619 (2011)
4. C. Li, M. Wang, J.F. Wu, *Opt. Lett.* **42**, 334 (2017)
5. Z. Wang, Y. Chong, J.D. Joannopoulos, M. Soljacic, *Nature* **461**, 772 (2009)
6. F.D.M. Haldane, S. Raghu, *Phys. Rev. Lett.* **100**, 013904 (2008)
7. Z. Yu, G. Veronis, Z. Wang, S. Fan, *Phys. Rev. Lett.* **100**, 023902 (2008)
8. M.Y. Wang, Y.S. Zhou, H.Y. Wang, *Opt. Commun.* **322**, 198 (2014)
9. R. Philip, M. Anija, C.S. Yelleswarapu, D.V.G.L.N. Rao, *Appl. Phys. Lett.* **91**, 141118 (2007)
10. E.N. Bulgakov, A.F. Sadreev, *Opt. Lett.* **39**, 1787 (2014)
11. K. Gallo, G. Assanto, K.R. Parameswaran, M.M. Fejer, *Appl. Phys. Lett.* **79**, 314 (2001)
12. B. Liu, Y.F. Liu, C. Jia, X.D. He, *AIP Adv.* **6**, 065316 (2016)
13. B. Liu, Y.F. Liu, S.J. Li, X.D. He, *Opt. Commun.* **368**, 7 (2016)
14. A. Alberucci, G. Assanto, *Opt. Lett.* **33**, 1641 (2008)
15. D.V. Novitsky, *Phys. Rev. A* **85**, 043813 (2012)
16. P.N. Melentiev, A.E. Afanasiev, A.S. Kalmykov, V.I. Balykin, *Eur. Phys. J. D* **71**, 152 (2017)
17. H. Ye, Z.Y. Yu, Y. Liu, Z.H. Chen, *Opt. Express* **24**, 24592 (2016)
18. H. Gao, Y.S. Zhou, Z.Y. Zheng, *J. Opt.* **18**, 105102 (2016)
19. X.S. Lin, J.H. Yan, L.J. Wu, S. Lan, *Opt. Express* **16**, 20949 (2008)
20. S. Feng, C. Ren, W.Z. Wang, Y.Q. Wang, *Opt. Commun.* **289**, 144 (2013)
21. J. Hwang, M.H. Song, B. Park, S. Nishimura, T. Toyooka, J.W. Wu, Y. Takanishi, K. Ishikawa, H. Takezoe, *Nat. Mater.* **4**, 383 (2005)
22. M.H. Song, B. Park, Y. Takanishi, K. Ishikawa, S. Nishimura, T. Toyooka, H. Takezoe, *Thin Solid Film* **509**, 49 (2006)
23. D. Jalas, A. Petrov, M. Eich, W. Freude, S. Fan, Z. Yu, R. Baets, M. Popović, A. Melloni, J.D. Joannopoulos, M. Vanwolleghem, C.R. Doerr, H. Renner, *Nat. Photonics* **7**, 579 (2013)

24. A. Kumar, T. Low, K.H. Fung, P. Avouris, N.X. Fang, *Nano Lett.* **15**, 3172 (2015)
25. P. Shekhar, J. Atkinson, Z. Jacob, *Nano Converg.* **1**, 14 (2014)
26. X.H. Wu, C.J. Fu, *AIP Adv.* **7**, 075208 (2017)
27. S. Dai, Z. Fei, Q. Ma, A.S. Rodin, M. Wagner, A.S. Mcleod, M.K. Liu, W. Gannett, W. Regan, K. Watanabe, T. Taniguchi, M. Thiemens, G. Dominguez, A.H.C. Neto, A. Zettl, F. Keilmann, P.J. Herrero, M.M. Fogler, D.N. Basov, *Science* **343**, 1125 (2014)
28. J.D. Caldwell, A.V. Kretinin, Y.G. Chen, V. Giannini, M.M. Fogler, Y. Francescato, C.T. Ellis, J.G. Tischler, C.R. Woods, A.J. Giles, M.H. Hong, K. Watanabe, T. Taniguchi, S.A. Maier, K.S. Novoselov, *Nature Commun.* **5**, 5221 (2014)
29. M.G. Moharam, D.A. Pommert, E.B. Grann, T.K. Gaylord, *J. Opt. Soc. Am. A* **12**, 1077 (1995)